# Kinetics of Aluminum-Water Split Reaction*

ABSTRACT

The energy producing aluminum-water split reaction is characterized experimentally using microcalorimetry. The rates of heat release during the reaction at two fixed temperatures, 303 and 313 K, were measured for spherical aluminum powders placed in liquid water. Fully and partially reacted powders were characterized using electron microscopy and x-ray diffraction. Experiments were performed with three commercial powders with nominal sizes of 3-4.5, 10-14, and 17-30 µm. The observed reaction could be broken down into several parts, including an induction time, two stages of relatively rapid reaction, and reaction termination. Initially, particles grow bayerite layers which later sinter together forming continuous aluminum-bayerite composites. The significance of the first of the rapid reaction stages increased for experiments at the higher temperature. It was also observed that finer powders exhibited a faster and more complete reaction. Experimental data were processed using a simplified kinetic model reported in the literature to assess the diffusion coefficient describing the reaction rate-limiting process: transport of hydroxo complexes of aluminum through a growing porous layer of bayerite. The calculated diffusion coefficient was in the range expected for the experimental temperatures. However, its dependence on the powder particle size and on the reaction time indicate that the current model is inadequate for describing the present experiments.

INTRODUCTION

Hydrogen is of interest for environmentally friendly energy storage and delivery [1-3]. It is particularly attractive when generated in-situ, e.g., via water split reaction, where a metal reacts with water. Current research is heavily focused on aluminum-water reactions [4-9]:

$$Al + 3H_2O \rightarrow Al(OH)_3 + 1.5H_2 \uparrow \qquad (1)$$
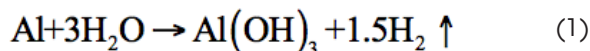
These reactions were shown to be economically attractive for pollution-free energy-generating technologies [10, 11]. However, the mechanisms affecting the reaction rates remain poorly understood.

In most experimental studies, the rate of reaction is monitored by tracking the amount of hydrogen released. Identification of kinetic trends from such measurements is difficult; changes in reaction rates can remain unnoticed or poorly resolved. Alternatively, measuring the heat release associated with the reaction using contemporary calorimetric techniques is possible with high resolution. The objective of this study is to characterize Al-water reaction using calorimetry and identify kinetic trends defining the reaction rate.

EXPERIMENTAL

Spherical aluminum powders from Alfa Aesar with nominal particle sizes 3-4.5 µm, 10-14 µm, and 17-30 µm were used. Particle size distributions were measured using a Beckman-Coulter LS230 Analyzer; respective volumetric average particle sizes were 7.2, 21.5, and 38.5 µm.

Isothermal heat flow calorimetry was carried out in a TA Instruments TAM III minicalorimeter (Multi 4mL). Measurements were performed at 303 and 313 K using a perfusion ampoule by TA Instruments. Samples were contained in 4-mL steel and glass reaction vessels. Measurement times ranged from hours to days. Fully and partially reacted samples were recovered for subsequent analysis by electron microscopy (SEM) and x-ray diffraction (XRD).

RESULTS

A pattern of heat release for Al reacting with liquid water is shown in Fig. 1. After an initial induction period, the main reaction proceeds in stages. Induction period is the time elapsed between the first contact between aluminum and water and the time the heat flow reached 1 % of its maximum value. The times τ_1 and τ_2 are defined as the times between the end of the induction period and the heat flow peak maxima of the first and second stages, respectively.
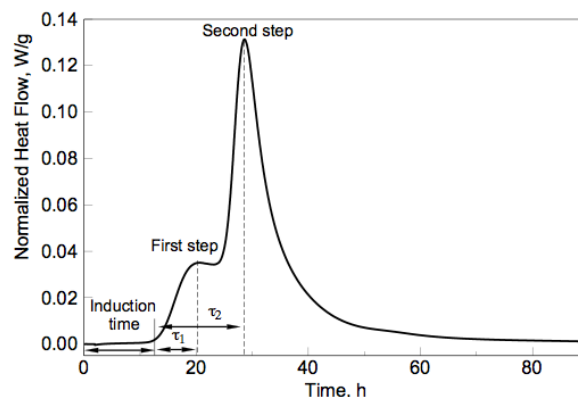

Figure 1: Normalized heat flow measured for 3-4.5 µm aluminum powder reacting with water at 303 K (30°C).

To evaluate the conversion completeness, the enthalpies were put in relation to the theoretical reaction enthalpy $\Delta H_{f,298}$ = −1293.1 kJ/mol [12].

Figure 2 shows XRD patterns of materials recovered after the induction period, after the first heat flow peak, and at the end of the measurement, respectively. No reaction product was detected after the induction period, and the only product at later stages is crystalline bayerite.
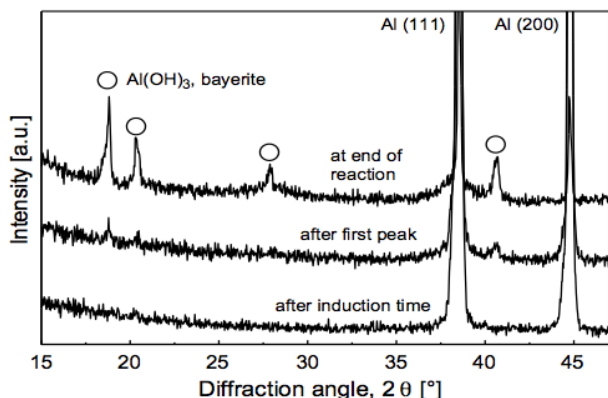

Figure 2: XRD patterns of samples recovered at different stages of the reaction at 303 K.

Figures 3 – 7 show backscattered electron images of the starting material, and of partially reacted materials.
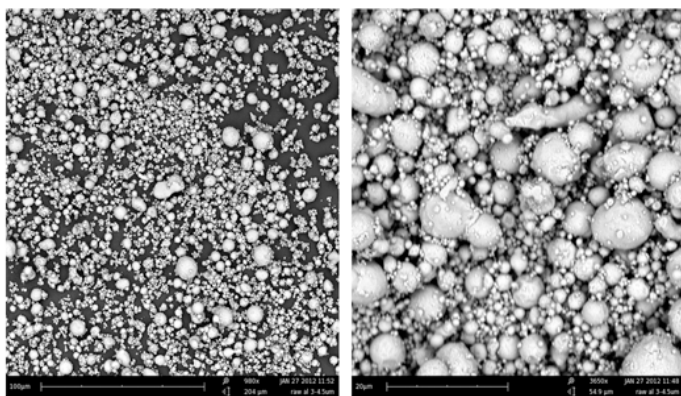

Figure 3: Starting material, 3-4.5 μm nominal particle size.

At the onset of the first reaction stage (Fig 4), the particle shape has changed slightly, although no grown surface layer can be seen. Particles show surface layers of bayerite after the first reaction step (Fig. 5). Particles deviate from the initial spherical shape, and the bayerite surface layers start forming bridges between particles. At the end of the measurement (Fig. 6), bayerite forms a continuous matrix with inclusions of remaining, unreacted aluminum. A brightness contrast within the bayerite matrix is seen clearly in Fig. 7. The fragment shown on the right, containing unreacted aluminum metal at its core shows an irregular outline and spherical inclusions with lower brightness near its perimeter. XRD shows no presence of any product phase other than bayerite, therefore the phase contrast must be the result of nanometer-scaled porosity. Thus, a first generation of dense bayerite cemented the aluminum particles together, while a slower reaction continued to consume aluminum while also dissolving and recrystallizing existing bayerite, forming a more porous second generation.
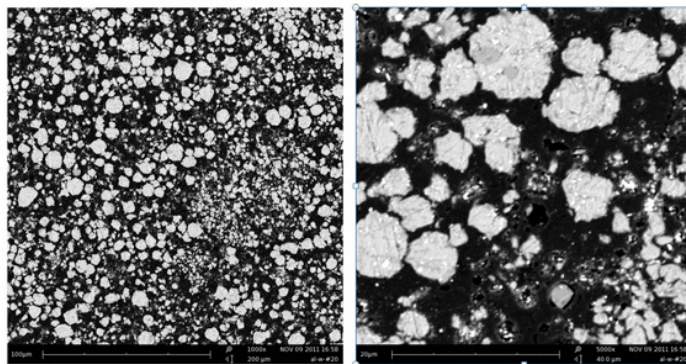

Figure 4: Al 3-4.5 μm, recovered after the induction period at 313 K (40 °C.)
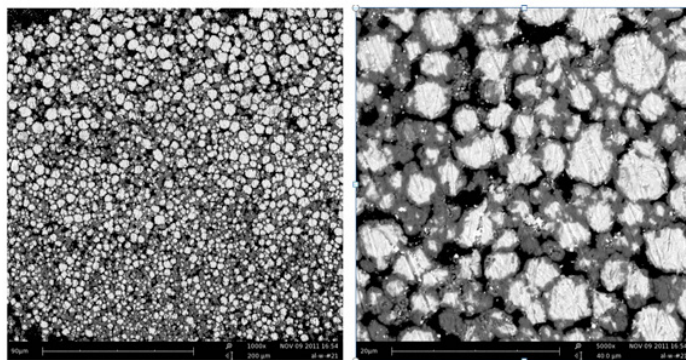

Figure 5: Al 3-4.5 μm, recovered after the first heat flow peak at 313 K (40 °C.)
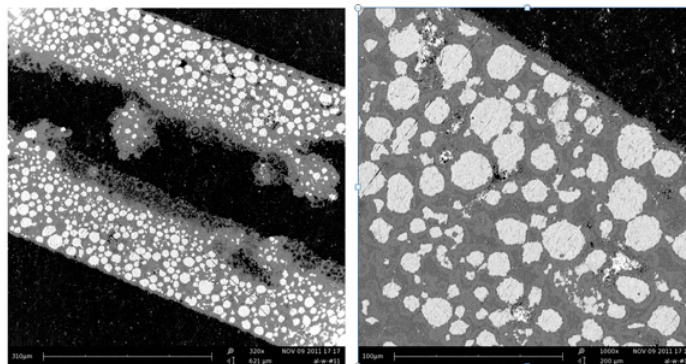

Figure 6: Al 3-4.5 μm at 313 K (40 °C), recovered after the reaction rate had slowed significantly, at 1300 min.
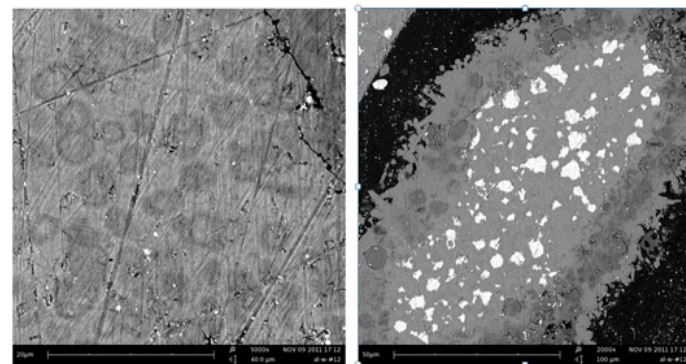

Figure 7: Al 10-14 μm at 313 K (40 °C), recovered after the reaction rate had slowed significantly, at 2680 min.

Figure 8 shows the effect of temperature on the reaction. All aspects of the reaction occur earlier at the higher temperature. At 313 K, the separation between first and second reaction steps is less pronounced, and the second reaction step is weaker relative to the first.
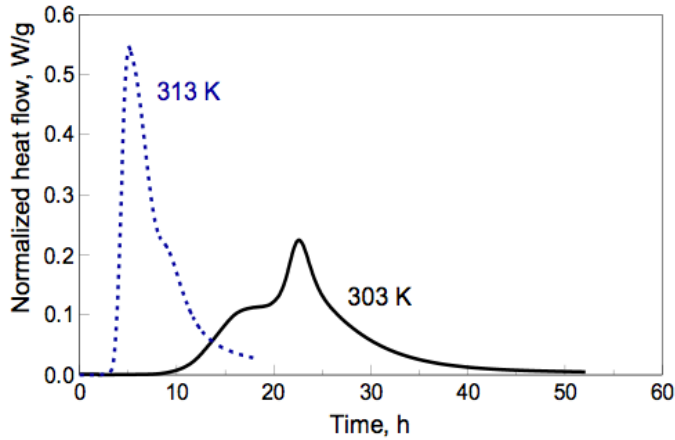

Figure 8: Normalized heat flow of the reaction of 3 – 4.5 µm aluminum with water at two different temperatures.

Figure 9 shows the effects of particle size. Larger particles show generally lower reaction rates. For larger particles, the first stage of the reaction becomes more prominent relative to the second stage, and the separation between the stages increases.
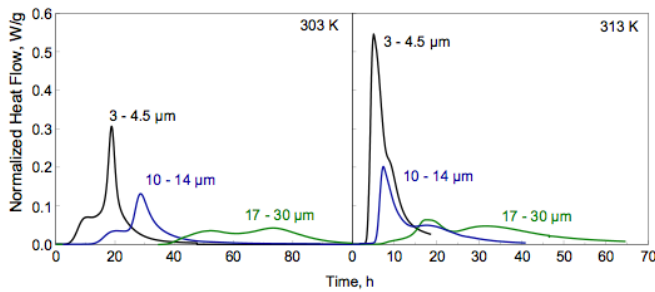

Figure 9: Normalized heat flows for the aluminum powders with different particle sizes reacting with water at different temperatures.

DISCUSSION

Induction Time

Amorphous alumina forms an amorphous hydrated gel as the first product of hydration [13]. The hydration rates observed in Ref. [13] at 298 K and 323 K agree with the induction periods observed in the present study. The hydration reaction is exothermic, but less than reaction (1). As the initial hydrated products form, the amorphous oxide layer likely becomes pitted and porous.

Fast Reaction

As Figs. 5 and 6 show, inter-particle contact is not extensive, and particles can be considered individually. The rate limiting process for the growth of a bayerite surface layer is the diffusion of the $Al(OH)_4^-$ complex [14] in liquid:

$$\alpha^2 = \frac{2.24 \rho_b^2 \upsilon D C_1 \sigma S_b V_b}{RT \rho_t^2 r^2} t \qquad (2)$$

where the α is the reaction completeness, $\rho_b = 2.42 \cdot 10^3$ kg/m³ and $\rho_t = 1.56 \cdot 10^3$ kg/m³ are respectively bulk density of bayerite and tap density of aluminum powder; $\upsilon = 0.5$ is a coefficient accounting for the growing bayerite porosity; $\sigma = 773 \cdot 10^{-3}$ J/m² is the surface energy at the solution/bayerite interface; $S_b = 53 \cdot 10^3$ m²/kg is the specific surface area of bayerite, $V_b = 32 \cdot 10^{-6}$ m³/mol is the molar volume of bayerite, $C_1 = 0.027$ kg/m³ [14] is the concentration of aluminum in solution, at the start of the hydrolytic polymerization reaction. r is the initial particle radius, R is the universal gas constant, T is temperature, t is time, and D is the diffusion coefficient. Based on experimental reaction times for 10-µm powders at 373 K, the diffusion coefficient was estimated in [14] to vary in the range of $(0.067 – 0.13) \cdot 10^{-10}$ m²/s. Eq. (2) was solved for the diffusion coefficient, D, and the reaction completeness was expressed through the measured rate of heat release, $\dot{Q}$:

$$\alpha = \frac{1}{Q_{complete}} \int_0^t \dot{Q} \, dt \qquad (3)$$

to yield:

$$D = \frac{RT \rho_t^2 r^2}{2.24 \rho_b^2 \upsilon C_1 \sigma S_b V_b t} \left(\frac{1}{Q_{complete}} \int_0^t \dot{Q} \, dt \right)^2 \qquad (4)$$

where $Q_{complete} = 15.42$ kJ/g is the theoretical maximum heat release expected upon the complete conversion of the entire powder mass load. Using experimental $\dot{Q}(t)$ curves, assessment of the diffusion coefficient is possible.

The time was set to zero at the end of the induction period for each experiment. The calculated values of the diffusion coefficient as a function of the reaction time are shown in Fig. 10 for the same experiments that were illustrated in Fig. 9.
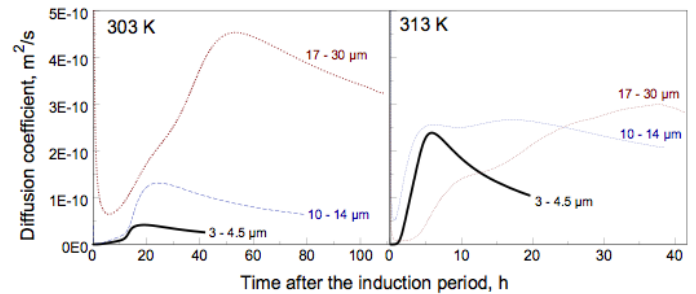

Figure 10: Diffusion coefficients for experimental runs illustrated in Fig. 9 calculated as a function of reaction time corrected for the induction period.

Generally, the range of values for D shown in Fig. 10 is higher than that reported by Rat'ko et al. [14], although more consistent with diffusion coefficients if ionic species in aqueous solutions.

Termination

The growing bayerite surface layers of adjacent particles form bridges and gradually fill all interstices between adjacent particles (see Figs. 6 and 7). The diffusion path between liquid solution and the surface of the remaining aluminum particles becomes longer until finally the reaction rate becomes too slow to detect.

Transition Stages

The transition between initial fast reaction and termination shows some systematic trends. At 303 K, two well-separated heat flow peaks are observed, which become more separated for larger particle sizes. At 313 K this separation is still observed, however the two heat flow peaks are less well resolved. Further, Figs 6 and 7 shows characteristic brightness contrasts in the bayerite. This could be related to the formation of several distinct generations of bayerite.

CONCLUSION

Reaction of aluminum with liquid water characterized by microcalorimetry includes several parts: induction time, two stages of relatively rapid reaction, and termination. The only reaction product formed at 303 and 313 K is bayerite. The significance of the first of the two rapid reaction stages increased in experiments at 313 K. Generally, finer powders were observed to react faster and to a greater completion. Effects of powder load and mass of water are found to be negligible. Reaction characteristics were poorly reproducible despite well maintained reaction temperatures. It is hypothesized that minor differences in powder packing and trapped gases could substantially affect reaction rates for the processes occurring directly on the particle surfaces, as expected for the alumina hydration occurring during the induction period. Processing the present experimental data using a simplified kinetic model available in the literature showed that the calculated diffusion coefficient for the rate-limiting process is affected by the reaction temperature, particle sizes, and reaction time. While the first effect is expected, the observed effects of particle size and reaction time likely indicate that the model is inadequate for describing the present experiments. Porosity of the growing bayerite, defining the rate of diffusion and thus the reaction rate, changes as a function of the reaction completeness. It is also affected by experimental conditions, including reaction temperature and powder particle size distribution.

ACKNOWLEDGEMENT

For more information or to place an order, go to http://www.tainstruments.com/ to locate your local sales office information.

REFERENCES

1. Crabtree GW, Dresselhaus MS, Buchanan MV. Physics Today. 2004;57:39-44.

2. Barreto L, Makihira A, Riahi K. International Journal of Hydrogen Energy. 2003;28:267-84.

3. Dunn S. Hydrogen futures: International Journal of Hydrogen Energy. 2002;27:235-64.

4. Wang W, Zhao XM, Chen DM, Yang K. International Journal of Hydrogen Energy. 2012;37:2187-94.

5. Wang HW, Chung HW, Teng HT, Cao G. International Journal of Hydrogen Energy. 2011;36:15136-44.

6. Deng ZY, Tang YB, Zhu LL, Sakka Y, Ye J. International Journal of Hydrogen Energy. 2010;35:9561-8.

7. Czech E, Troczynski T. International Journal of Hydrogen Energy. 2010;35:1029-37.

8. Bunker CE, Smith MJ, Shiral Fernando KA, Harruff BA, Lewis WK, Gord JR, et al. ACS Applied Materials and Interfaces. 2010;2:11-4.

9. Deng ZY, Ferreira JMF, Sakka Y. Journal of the American Ceramic Society. 2008;91:3825-34.

10. Franzoni F, Mercati S, Milani M, Montorsi L. International Journal of Hydrogen Energy. 2011;36:2803-16.

11. Franzoni F, Milani M, Montorsi L, Golovitchev V. International Journal of Hydrogen Energy. 2010;35:1548-59.

12. Robie RA, Hemingway BS. US Geological Survey Bulletin. 1995;2131.

13. Miśta W, Wrzyszcz J. Thermochimica Acta. 1999;331:67-72.

14. Rat'ko AI, Romanenkov VE, Bolotnikova EV, Krupen'kina ZV. Kinetics and Catalysis. 2004;45:149-55.